

Flow focusing in microchannels

M. R. Davidson* D. J. E. Harvie* J. J. Cooper-White†

(Received 16 November 2004, revised 11 February 2005)

Abstract

A volume-of-fluid numerical method is used to predict the dynamics of drop formation in an axi-symmetric microfluidic flow-focusing geometry for a liquid-liquid system. The Reynolds numbers and Weber numbers approximate those of a three-dimensional flow in recently published experiments. We compare the predicted drop formation with the experimental results at various flow rates, and discuss the mechanisms of drop formation in this context. Despite the differences in geometry, we find qualitative correspondence between the numerical and experimental results. Both end-pinching and capillary-wave instability are important for droplet break-up at the higher flow rates.

*Department of Chemical and Biomolecular Engineering, The University of Melbourne, Parkville, Victoria 3010, AUSTRALIA. <mailto:m.davidson@unimelb.edu.au>

†Department of Chemical Engineering, The University of Queensland, St. Lucia, Queensland 4067, AUSTRALIA.

See <http://anziamj.austms.org.au/V46/CTAC2004/Davi> for this article, © Austral. Mathematical Soc. 2005. Published 14 March 2005, amended March 18, 2005. ISSN 1446-8735

Contents

1 Introduction	C48
2 Formulation	C49
3 Results and Discussion	C51
4 Conclusion	C57
References	C57

1 Introduction

The continuous manufacture of emulsions which have defined micron scale droplet sizes are paramount to the successful market acceptance of many products within the food, cosmetic, pharmaceutical and photographic industries. An understanding of the deformation history and breakage of drops of one liquid within another liquid is thus of vital importance. Flow focusing of a continuous stream of liquid is one way of creating such drops. In this procedure the drop liquid flows as a stream in the middle of a channel and is surrounded by a second immiscible liquid flow. Both liquids are forced to flow through a small calibre contraction or orifice located downstream. The flow rate of the surrounding fluid is typically greater than that of the droplet stream which is consequently forced into a thin filament within or downstream of the contraction where it breaks into droplets. The method offers a high degree of control over the velocity gradients experienced by the fluid to be dispersed and is suitable for use at the micron scale.

Very few studies have been published on flow focusing induced liquid droplet formation and there appears to be no numerical modelling of it. Experiments have demonstrated the use of flow focusing to create monodis-

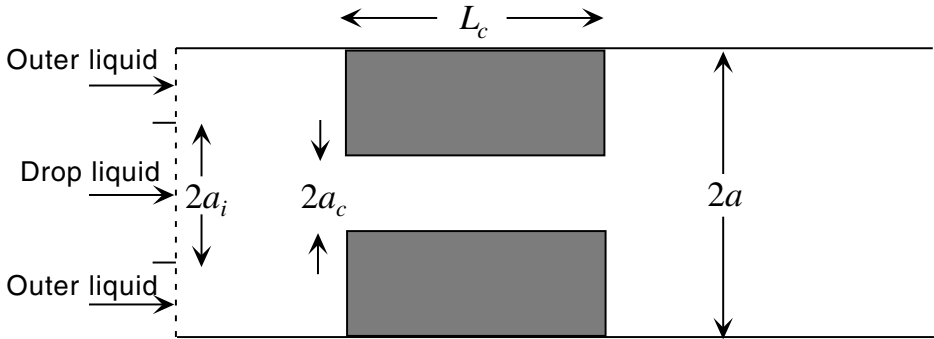


FIGURE 1: Cylindrical flow geometry.

persed micron sized droplets in a gas stream [3] and bubbles in a liquid stream [4]. Nisisako et al. [5] demonstrated a method for generating droplets in a liquid at a micro-sized T-junction. Anna et al. [1] presented a range of droplet formation behaviour from experiments in a microfluidic flow-focusing device of rectangular cross-section in which the inner and outer streams were water and oil, respectively. In this paper, numerical simulations of two-dimensional axi-symmetric flow focusing are undertaken for conditions approximating those of the three-dimensional flow in [1]. The calculations use a volume-of-fluid (VOF) finite volume technique. The predicted drop formation is compared qualitatively with the experimental results at various flow rates, and the mechanisms of drop formation in this context are discussed.

2 Formulation

Consider a cylindrical pipe of radius a containing an abrupt cylindrical contraction of radius a_c and length L_c (Figure 1). Two coaxial immiscible liquid streams enter the cylinder through $0 \leq r \leq a_i$ (inner stream) and $a_i < r \leq a$ (outer stream) with mean inner and outer velocities \bar{V}_i and \bar{V}_o , respectively. Hereafter, subscripts i and o denote the inner and outer fluids, respectively.

The axi-symmetric evolution of the interface between these two streams is investigated from an initial state in which the flow geometry is initially completely filled with outer fluid. We assume that the interface never attaches to the channel walls (that is, the wall is non-wetting with regard to the inner fluid) since that appears to be the case in the experiments of Anna et al. [1].

In terms of dimensionless velocity, length and time, scaled according to \bar{V}_i , a and a/\bar{V}_i , respectively, the equations of motion for a VOF calculation are

$$\frac{\partial C}{\partial t} + \nabla \cdot (\mathbf{U}C) = 0, \quad (1)$$

$$\frac{\partial \rho \mathbf{U}}{\partial t} + \nabla \cdot (\rho \mathbf{U} \mathbf{U}) = -\nabla P + \frac{1}{\text{We}} \mathbf{F}_S + \frac{1}{\text{Re}} \nabla \cdot \boldsymbol{\tau}, \quad (2)$$

$$\nabla \cdot \mathbf{U} = 0, \quad (3)$$

$$\rho = \rho_i C + \rho_o (1 - C), \quad (4)$$

where C is a fractional volume function, P denotes pressure, $\boldsymbol{\tau}$ is the viscous stress tensor and \mathbf{F}_S is the surface force arising from interfacial effects. The gravitational force has been ignored as it is negligible compared with the surface force at the micron scale. The fractional volume function C is advected with the local velocity \mathbf{U} . The above equations correspond to the flow of a mixture with variable properties (density ρ and viscosity μ), combined with advection of the volume fraction. The mixture takes the local fluid properties, with a volume fraction weighted average in computational cells containing the interface. The density and viscosity are obtained according to Equation (4). The interface position is determined implicitly at any time by consideration of the volume fraction distribution.

The dimensionless parameters in Equations (1-3) are the Weber and Reynolds numbers,

$$\text{We} = \frac{\rho_r \bar{V}_i^2 a}{\sigma}, \quad \text{Re} = \frac{\rho_r \bar{V}_i a}{\mu_r}, \quad (5)$$

respectively, where ρ_r and μ_r denote reference values of density and viscosity, respectively, and σ is the coefficient of interfacial tension between the two

liquids. Here, the density and viscosity of the inner fluid are the reference values.

The VOF algorithm of Rudman [7], modified to ensure that the interface never attaches to the wall, is used to solve Equations (1–3). The method to advect C is based on the volume tracking method of Youngs [10] as described in [7]. The surface force \mathbf{F}_S is represented using Rudman’s improved implementation [7] of the CSF method [2]. Axi-symmetric flow calculations are performed in cylindrical polar coordinates on the symmetric half of a computational domain with 64 mesh cells spanning the cylinder radius a . The radial velocity in the leftmost row of cells at flow entry is set to zero to numerically pin the contact line between the two fluids at the entrance. Each stream is assumed to enter the flow domain with a uniform velocity profile. The choice of velocity profile is not expected to be important for the low Reynolds numbers encountered in micro-channel flow. The length of the domain is chosen to be $5a$ or $10a$, depending on the distance required for droplets to form. Increasing the number of cells in each direction by 50 per cent resulted in calculated interfaces which were almost coincident in test cases, with minor differences sometimes occurring close to droplet pinch-off. Further grid refinement was not practical because the computation time required exceeds the resources available.

3 Results and Discussion

A 1:4 contraction ($a_c/a = 0.25$) of length $L_c/a = 1.25$, located at one cylinder radius downstream, is considered. The entry radius of drop liquid is taken to be $a_i/a = 0.5$. The flow focusing experiments of Anna et al. [1] in micro-channels of rectangular cross-section are the guide for the present choice of flow parameters. In that experiment, water drops are formed in oil laden with surfactant for which $\rho_o/\rho_i = 0.9$ and $\mu_o/\mu_i = 6$. Values of the Reynolds and Weber numbers (Eqn. 5) are chosen so that corresponding values based

on velocity and radius in the contraction are the same as those in the orifice of the experiment [1]. In evaluating these parameters it is assumed that $a = 80 \mu\text{m}$ and $\sigma = 0.01 \text{ N/m}$. For the experiment, the Ohnesorge number $\text{Oh} = \text{We}^{1/2}/\text{Re}$ is fixed as it depends only on the fluid properties and the length scale. For the present calculations $\text{Oh} = \mu_i/(\rho_i\sigma a)^{1/2} = 0.033$.

Figure 2 shows selected drop breakup sequences when the ratio of volumetric flow rates of the inner and outer streams $Q_i/Q_o = 0.25$. Figure 3 shows corresponding results for $Q_i/Q_o = 0.025$. The labels (c), (d), (f) in Figure 2, and (i), (j), (l) in Figure 3 correspond to cases so labelled in the experiment in so far as the Reynolds and Weber numbers local to the contraction are the same as in the experiment. Other such cases were also simulated but are not presented here. The description of experimental results by Anna et al. [1] is somewhat sketchy but they do report breakup within the orifice for Case (i) when $Q_i/Q_o = 0.025$ and for a case corresponding to $\text{Re} = 0.089$ and $\text{We} = 0.87 \times 10^{-5}$ (lower than in Case (c)) when $Q_i/Q_o = 0.25$. Here, breakup is predicted within the contraction for both Cases (c) and (i).

We explain the breakup in Cases (c) and (i) as follows: In both cases the effect of interfacial tension is so large that the inner fluid almost completely fills the width of the contraction in a capsule-like formation. Consequently the outer fluid, which has the greater flow rate, must flow along a thin annular region close to the wall. This results in a large axial drag which accelerates the inner liquid within the contraction until its flow rate therein exceeds the fixed rate of supply from the cylinder inlet. This causes a neck to form followed by breakup in a manner analogous to breakup of a pendant drop under a gravitational force. We refer to this as drag-induced breakup. The detached fluid capsule (drop) rapidly assumes a spherical shape as it clears the end of the contraction, again because of the high interfacial tension forces.

Anna et al. [1] report the formation of drops approximately the size of the orifice for Cases (c) and (d); however, inspection of the images in their phase diagram of drop formation suggests the drops are somewhat larger than the orifice diameter, similar to that predicted here. Smaller drops were observed

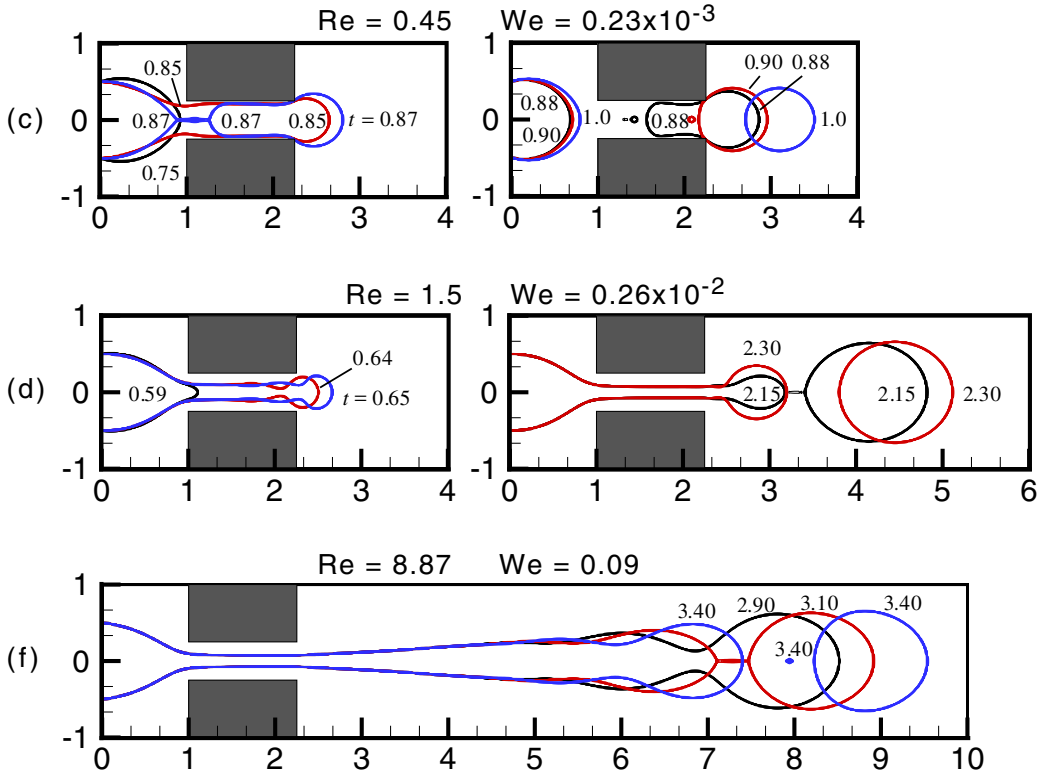


FIGURE 2: Selected drop breakup sequences for stream flow rate ratio $Q_i/Q_o = 0.25$. The Cases (c), (d) and (f) correspond roughly to cases so labeled in Figure 3 of [1]. View the animation movies for [Case \(c\)](#), [Case \(d\)](#) and [Case \(f\)](#) by clicking on these names.

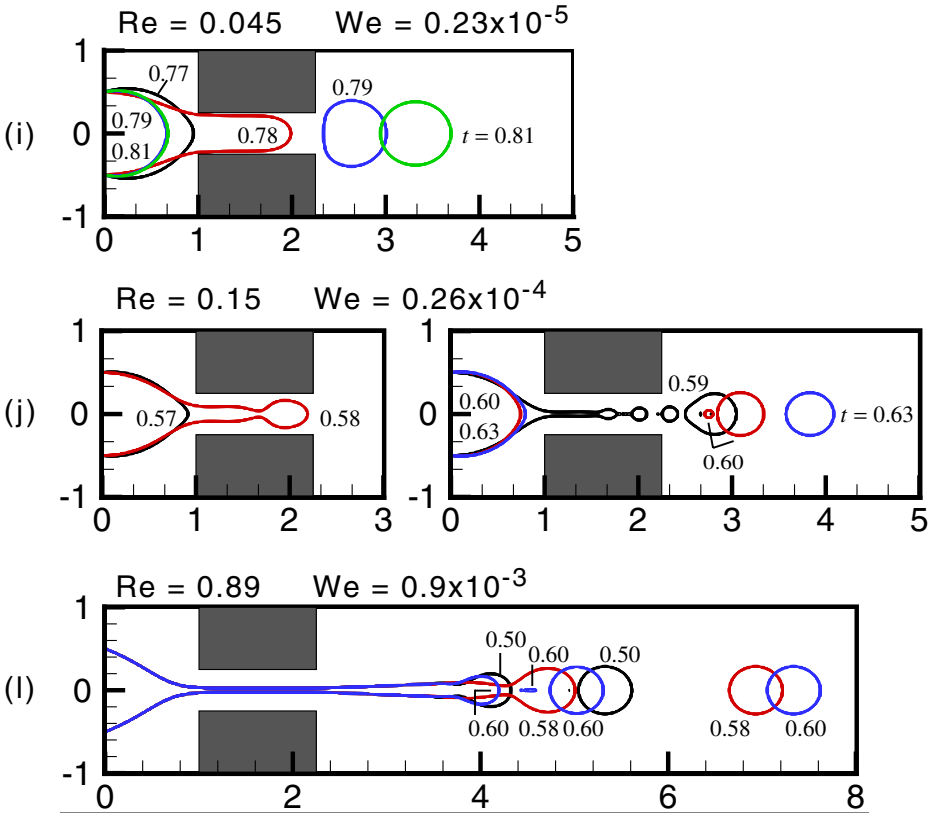


FIGURE 3: Selected drop breakup sequences for stream flow rate ratio $Q_i/Q_o = 0.025$. The Cases (i), (j) and (l) correspond roughly to cases so labeled in Figure 3 of [1]. View the animation movies for [Case \(i\)](#), [Case \(j\)](#) and [Case \(l\)](#) by clicking on these names.

by Anna et al. for the lower flow ratio $Q_i/Q_o = 0.025$ and this effect is replicated here in the predictions (Figure 3). Also observed experimentally was the formation of a small satellite drop in Cases (i) and (j). This is also predicted here but the satellite subsequently coalesces with the primary drop in each case. This occurs because the primary drop moves more slowly than the continuous phase, whereas the much smaller satellite drop almost matches the continuous phase velocity. Multiple smaller drops were observed for Case (l) but only a single satellite is predicted. A satellite drop is also predicted for Case (f). However, the calculations for (f) and (l) do not proceed far enough to show coalescence. Anna et al. observe the formation of both monodisperse and polydisperse droplets, with higher Reynolds and Weber numbers and lower Q_i/Q_o values favouring the polydisperse regime. In contrast, a feature of every prediction here is the repeated formation at regular intervals of identical drops (apart from small satellite drops); this is more apparent in the animations.

In Cases (d), (f) and (l), breakup occurs in the expansion downstream of the contraction and factors other than drag can be important in that event. One of these is the phenomenon of end-pinching (Stone et al. [8], Stone and Leal [9]) which can occur when the stretching of a fluid thread is abruptly stopped as occurs (approximately) when the drop fluid exits the contraction and enters the expansion. As explained in [8] and [9] interfacial tension causes the end of the drop fluid to form a bulb; a waist then forms behind it leading to a localised pressure increase there and a consequent pressure driven flow out of the waist or neck which eventually pinches off. This process is opposed by flow out of the bulb (resulting from a pressure increase therein due to bulb curvature) which favours the retraction of the bulb towards the neck region (see also [6]).

Capillary-wave instability may also be important in Cases (d), (f) and (l). Stone and Leal [9] report growth times for various initial disturbance amplitudes on an infinite stationary fluid cylinder in a second otherwise stationary fluid. The values given are the times for a capillary wave to grow to half

the cylinder radius. In terms of the present scaling, the dimensionless capillary growth times for an inner/outer fluid viscosity ratio of 0.1 (compared with 0.17 in the present calculations) are found to be in the ranges 0.06–0.28, 0.36–1.6 and 0.036–0.16 for Cases (d), (f) and (l), respectively. These are less than or are comparable to the corresponding dimensionless times (1.49, 2.68, 0.16) to breakup measured from when the drop fluid enters the expansion (leaves the contraction). Consequently, we expect capillary-wave instability as well as end-pinching to contribute to breakup in these cases. Indeed, capillary waves are visible behind the bulb in Cases (d) and (f), and to a lesser extent in (l).

Like Cases (c) and (i), Case (j) in Figure 3 also show breakup within the contraction. Necking first occurs within the contraction (see for example $t = 0.58$) and this is thought to be an incipient drag-induced breakup event. However, breakup occurs right at the end of the contraction (beginning of an expansion) so end-pinching seems likely to be an important effect in Case (j). The occurrence of multiple necking prior to breakup suggests that capillary-wave instability also plays a role. Indeed, the capillary growth time, as calculated above, ranges from 0.006 to 0.027, and Figure 3 suggests that the primary drop breaks off at a time less than 0.01 after reaching the end of the contraction. This suggests that the capillary growth time is comparable to the time to achieve end-pinching in this case as well.

Figures 2 and 3 each show the effect of increasing total flow rate, but at two different inner/outer flow ratios. Cases (c) and (i), which have the lowest total flow rates presented here, show a capsule-like formation within the contraction because of the dominating effect of interfacial tension, as discussed above. As the overall flow rate increases, the inner fluid reaches the contraction more quickly as is expected. Cases (d) and (f) both show the bulb behind the thread connecting the primary drop prior to pinch-off. The rear bulb is more elongated in Case (f) than in Case (d) because interfacial tension effects are less at the larger flow rate. Bulb formation behind the neck is barely visible in Case (l) of Figure 3. Presumably this occurs because

the outer/inner flow ratio in Figure 3 is much larger (leading to greater shear rates) than in Figure 2. For the same reason, the inner fluid stream is stretched thinner in Cases (j) and (l) than their Figure 2 counterparts (d) and (f).

4 Conclusion

A volume-of-fluid numerical method has been used to predict the shape evolution of the interface between two immiscible liquid streams, directed concentrically into a cylinder containing a 4:1 contraction of diameter. Predictions are based on Reynolds and Weber numbers in the contraction which are the same as those for the microfluidic flow focusing experiments of [1]. The experimental flow field is three-dimensional in a device with rectangular cross-section, whereas the numerical calculations are for axisymmetric flow in a geometry of cylindrical cross-section. Despite the differences in geometries, qualitative correspondence is found between the theoretical and experimental results. We conclude that the mechanisms for droplet breakup range from drag-induced at the lowest flow rates when breakup occurs inside the contraction, to end-pinching and capillary-wave instability at higher flow rates when breakup occurs downstream of the contraction.

Acknowledgments: This research was supported by the Australian Research Council Linkage Grants Scheme.

References

- [1] S. L. Anna, N. Bontoux, and H. A. Stone. Formation of dispersions using “flow focusing” in microchannels. *Appl. Phys. Lett.*,

- 82(3):364–366, 2003. C49, C50, C51, C52, C53, C54, C57
- [2] J.U. Brackbill, D.B. Kothe, and C. Zemach. A continuum method for modelling surface tension. *J. Comput. Phys.*, 100:335–354, 1992. C51
- [3] A. M. Ganan-Calvo. Generation of steady liquid microthreads and micron-sized monodisperse sprays in gas streams. *Phys. Rev. Lett.*, 80(2):285–288, 1998. C49
- [4] P. Garstecki, I. Gitlin, W. DiLuzio, G.M. Whitesides, E. Kumacheva, and H.A. Stone. Formation of monodisperse bubbles in a microfluidic flow-focusing device. *Appl. Phys. Lett.*, 85(13):2649–2651, 2004. C49
- [5] T. Nisisako, T. Torii and T. Higuchi. Droplet formation in a microchannel network. *Lab. Chip*, 2:24–26, 2002. C49
- [6] T.R. Powers, D. Zhang, R.E. Goldstein and H.A. Stone. Propagation of a topological transition: The Rayleigh instability. *Physics of Fluids*, 10(5):1052–1057, 1998. C55
- [7] M. Rudman. A volume tracking method for interfacial flows with large density variations. *Int. J. Numer. Meth. Fluids*, 28:357–378, 1998. C51
- [8] H. A. Stone, B.J. Bentley and L.G. Leal. An experimental study of transient effects in the breakup of viscous fluids. *J. Fluid Mech.*, 173:131–158, 1986. C55
- [9] H. A. Stone and L.G. Leal. Relaxation and breakup of an initially extended drop in an otherwise quiescent fluid. *J. Fluid Mech.*, 198:399–427, 1989. C55
- [10] D.L. Youngs. Time-dependent multi-material flow with large fluid distortion, in K.W. Morton and M.J. Baines (eds.), *Numerical Methods for Fluid Dynamics*, pp. 273–285, Academic Press, New York, 1982. C51